

Performance analysis of microwave carrier for K_u-band satellite signal

M. R. H. Khan^{*,†}, M. F. Islam[†], G. Sarowar[†], T. Reza[†] and M. A. Hoque

rhkhan@iut-dhaka.edu fokhrul@iut-dhaka.edu asim@iut-dhaka.edu taslim@iut-dhaka.edu
mahoque@iut-dhaka.edu

[†]Islamic University of Technology, Dhaka, Gazipur 1704, Bangladesh.

^{*}Centre for Telematics and Information Technology (CTIT), Telecommunication Engineering group, Faculty of EEMCS, University of Twente, PO Box 217, 7500 AE Enschede, The Netherlands.

Summary

The system analysis and the experimental demonstration of an optically generated microwave carrier signal by heterodyning of two lasers is described in this paper. The carrier signal is used for downconversion of the K_u-band (10.7–12.75 GHz) satellite signal received from a phased array antenna (PAA) of a DVB-S (Digital Video Broadcasting-Satellite) system. The impact of the laser parameters (i.e., optical power and linewidth) on the quality of the generated carrier (i.e., phase stability and carrier-to-noise ratio) is analyzed for a 25×64 elements PAA system. It is experimentally demonstrated that, in order to have an optically generated carrier to meet the required performance for the K_u-band satellite reception, the lasers linewidth should be in the order of tens of Hz, with a maximum relative intensity noise (RIN) of -123 dB/Hz and a minimum optical power of 3.1 mW. An optical frequency locked loop (OFLL) to stabilize the generated carrier is also implemented. The carrier is stabilized within the maximum allowable ±4 MHz drift by using the proposed OFLL and gives a loop settling time of 11.5 μs.

Key words:

phased array antenna, optical heterodyning, carrier generation, K_u-band satellite signal, laser linewidth, stability, optical frequency locked loop (OFLL).

1. Introduction

In the last few years an increasing interest has been addressed on application of phased array antenna (PAA) to many satellite services ranging from digital radio and TV broadcast to broadband internet services [1], [2]. Potential applications especially regard mobile environments (cars, trains, boats, airplanes). A PAA is a set of multiple antennas, called antenna element (AE). Modern PAA consists of a large number of small antenna elements (AEs) and it can achieve the same gain of a large mechanically steerable antenna [3]. Recently, the use and advantages of PAA system for satellite communications systems have been thoroughly described in literature [4], [5], [6]. When installed on a vehicle a PAA system can be an advantageous solution for receiving satellite signals due to the flatness of its shape hence provides low aerodynamic profile [2] and to the fact that it can be electronically beamsteered, not requiring continuous mechanical realignment. Additional to that are the

possibilities for beam-shaping, tracking and multi-beam reception [7]. The satellite signal received by the AE of the PAA is downconverted into lower frequency to ease on amplification and further processing. Downconversion is done by mixing the received signal with a carrier signal at an RF mixer placed at each AE. To maintain phase synchronization among the carrier signals, the distribution of carrier signal from a central source is essential. The distribution of carrier signal by means of coaxial cable or waveguide is limited by the transmission line losses and their bulk size. Photonics offer an interesting alternative because these systems take advantage of the extremely low transmission and distribution losses (0.2 dB/km) of the standard single-mode fiber (SMF). In addition to that, optical fiber cables are compact, lightweight and provide wide bandwidth and immunity to electromagnetic interference [8]. This approach has been proven as a successful solution in many deployed systems for instance radio-astronomy [9], [10] and satellites for remote sensing [11]. In order to use an optically generated carrier in a satellite reception system it must meet the criteria of that of the specifications given for commercially available electronic carrier. The crucial challenge for optically generated carrier is to meet the requirements in term of low phase noise, low drift, carrier-to-noise ratio (CNR) and wide tunability [12]. Various approaches to generate an carrier signal using optical techniques have recently been reported [13], [14], [15]. Several approaches being investigated includes carrier signal generation by external modulation [13], mode locked lasers [14], and optical heterodyning using two lasers [15]. Methods based on external modulation generates carrier with low phase but need components such as filters to select the desired optical sidebands in order to obtain an carrier signal. This method works well for applications requiring fixed frequency carrier. The main disadvantage is that to generate a tunable carrier the notch filter has to be tunable and hence put complexity on the system. Also, lasers having high frequency drift can no use in this scheme. Moreover, output power of the generated carrier is low due to carrier suppression in the notch filter. Mode-locked lasers generate optical carrier signals with relatively low phase noise [16]. However, mode-locked lasers are

sensitive to the environment variation including temperature fluctuation and vibrations. Therefore, a complex feedback system for long term stabilization is usually required [17]. carrier generation based on optical heterodyning techniques where a beat signal is generated from the mixing of two light sources can be interesting solution due to ease on tunability. The frequency of the generated carrier is nothing but the frequency difference of two lasers. The free running heterodyning scheme benefits with a very wide tuning capability and the generated carrier can be freely adjusted [15]. However, the drawbacks come in the form of frequency drift. Among various methods proposed so far to stabilize the generated carrier, one of the most exploited techniques is the one known as optical phased locked loop (OPLL). In an OPLL the rate at which the relative phase between two heterodyned lasers changes is locked to a reference RF signal [18]. Nevertheless, OPLL significantly increases system complexity and cost which burden the implementation in many applications [19]. However, in various applications phase coherence between the two lasers is not necessary. A laser having ultra-narrow linewidth relaxes the stringent linewidth requirements for optically generated carrier. In that case an optical frequency locked loop (OFLL) [20] consisting of a so-called slave laser maintaining a highly precise frequency offset from a reference, labeled as master laser, would serve the requirements. In this paper an optically generated carrier based on heterodyning of a pair of distributed-feedback (DFB) lasers [21] are considered. Here an efficient technique to lock two lasers at any fixed frequency difference is presented. This approach is promising in terms of compactness, low phase noise and high stability. This paper demonstrates the feasibility of such a system to provide carrier signals. The remainder of the paper is organized as follows. Section II describes the theory of photonic carrier generation by optical heterodyning. In Section III, the proposed optically generated carrier for PAA system is described. In Section IV, the photonic carrier generation criteria namely the linewidth requirements and CNR criteria are presented. Section V demonstrates the stabilization of optically generated carrier. In the last section, the conclusions of this analysis are stated.

2. Photonic Carrier Signal Generation by Heterodyning

Let us consider two lasers L_1 and L_2 at frequencies f_{L1} and f_{L2} , respectively. These two laser signals with the same polarization are combined. A beat signal is created at the output of the photodetector. In the absence of frequency noise, the photodetector output current, $I(t)$, is a sinusoidal signal with a frequency equal to the frequency difference

between the two lasers, $f_{LO} = f_{L1} - f_{L2}$. The electric fields from each of the lasers are given by

$$E_{L1}(t) = E_{01} \exp(j[2\pi f_{L1}t + \phi_1(t)]) \quad (1)$$

$$E_{L2}(t) = E_{02} \exp(j[2\pi f_{L2}t + \phi_2(t)]) \quad (2)$$

where $\phi_1(t)$ and $\phi_2(t)$ represent the phase noise of the laser lights. The output current from the detector can be expressed as [22]

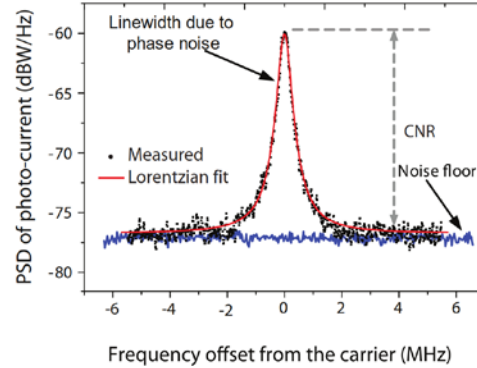


Fig. 1: PSD of photodetector output.

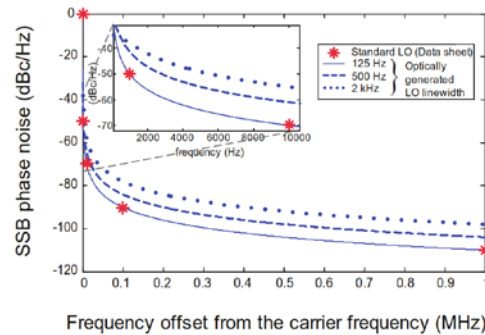


Fig. 2. SSB phase noise for various linewidths of the optically generated carrier.

$$I(t) = r_{pd} (P_{L1} + P_{L2}) + 2r_{pd} \sqrt{P_{L1}P_{L2}} \cos[2\pi f_{LO}t + \phi_{LO}] \quad (3)$$

where r_{pd} is the responsivity of the photodetector. The phase variation $\phi_{LO} = \phi_1(t) - \phi_2(t)$ is the difference of the independent phase variations of the individual lasers and $2r_{pd} \sqrt{P_{L1}P_{L2}}$ is the amplitude of the generated carrier. The power spectral density (PSD) of the photodetector output current, $I(t)$ is expressed as [23], [22]

$$S_I(f) = 2r_{pd}^2 P_{L1} P_{L2} \frac{1 / \pi \Delta \nu_{LO}}{1 + \left[\frac{2(f - f_{LO})}{\Delta \nu_{LO}} \right]^2} \quad (4)$$

where the beat linewidth of the optical carrier, $\Delta \nu_{LO} = \Delta \nu_1 + \Delta \nu_2$ is equal to the sum of the two linewidths of the lasers [24], [25]. The PSD of the optically generated carrier is a Lorentzian centered at f_{LO} . Due to the laser phase noise, the spectral linewidth of the laser broadens into a Lorentzian shape and ultimately broadens the

optical carrier linewidth. The function in Equation (4) is plotted in Figure 1, for a value of optical carrier linewidth, Δf_{LO} , of 1 MHz and it gives a Lorentzian shape centered at f_{LO} . The two lasers used for the optical heterodyning are a DFB laser (Avanex Inc., A1905LMI) and a tunable laser diode (TLD, Santec TSL210). In Figure 1, the black dots show the measured RF beat spectrum and the red line shows a Lorentzian fit with a -3 dB linewidth of 1 MHz. The noise floor is measured when no optical power is applied to the PD.

The RF power of the carrier signal delivered to a load can be calculated using the following equation:

$$P_{LO} = \langle I_{LO}^2(t) \rangle R_L = \frac{1}{2} \left(2r_{pd} \sqrt{P_{L1} P_{L2}} \right)^2 R_L = \frac{1}{2} I_{av}^2 R_L \quad (5)$$

where the symbol $\langle \bullet \rangle$ denotes average, I_{LO} and R_L are the current and load impedance at the output of the PD, respectively, and I_{av} is the average photo-current expressed as:

$$I_{av} = r_{pd} P_T = r_{pd} (P_{L1} + P_{L2}) = 2r_{pd} P_L \quad (6)$$

3. System Description

The block diagram of the proposed antenna system using an optically generated carrier is presented in Figure 3. Since the received signal power density from the satellite is relatively low, the antenna should have a high gain and a low noise temperature to achieve the required CNR for K_u -band satellite signals. This dictates a number of antenna elements of at least 1600 [1]. Those can be placed as 25 tiles of 64 AEs. More details of this PAA system have been described in [1]. In this paper we restrict

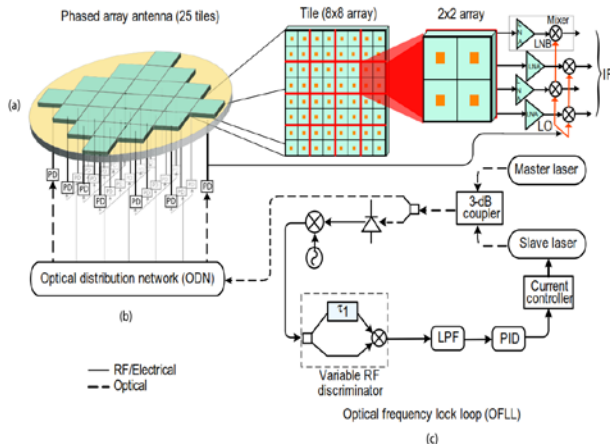


Fig. 3. Proposed K_u -band PAA down-conversion system using an optically generated carrier. (a) phased array antenna structure; (b) optical distribution network (ODN); (c) optical heterodyning system.

LNA: low noise amplifier, LNB: low noise block, LPF: low pass filter.

ourselves to the downconversion system of the DVB-S reception. The proposed downconversion system consists

of a PAA, an optical distribution network (ODN) and the optical heterodyning scheme. As a basic building block, an 8×8 antenna tile consisting of 64 antenna elements (AEs) is considered, shown in Figure 3(a). The DVB-S signal received by each AE will be amplified by a low noise amplifier (LNA) and downconverted at the mixer using a centrally generated carrier signal.

The carrier is generated optically and also distributed by an optical distribution network (ODN) in order to take advantage of low loss distribution by means of standard single-mode fiber. Shown in Figure 3(b), the ODN is implemented in conjunction with an individual photodetector (PD) at each antenna tile. The carrier signal at the output of each PD is then distributed to each mixer. The optical heterodyning system that generates the carrier signal is shown in Figure 3(c). The lasers are oscillating with a frequency difference chosen to produce 9.75 GHz or 10.6 GHz carrier signal at the output of the PDs. This enables downconversion of the upper or lower sideband of the 10.7 GHz to 12.75 GHz DVB-S signal to a required intermediate frequency (IF) in the L band (950 MHz – 2150 MHz). The frequency stabilization of the optically generated carrier is accomplished by an optical frequency lock loop (OFL) explained in detail in Section V.

4. Criteria for the optically generated carrier

In order to use the optically generated carrier in a DVB-S system its performance must meet the criteria for power, phase noise and frequency stability. The parameter values that are useful for our analysis are taken from the DVB-S standard [26], specifically the phase noise values shown in Table 1.

Table 1: LO specification for DVB-S receiver

Carrier Parameters	Values
Frequency range	9.75 GHz or 10.6 GHz
Single sideband (SSB) phase noise	-50 dBc/Hz @ 1 kHz -70 dBc/Hz @ 10 kHz -90 dBc/Hz @ 100 kHz -110 dBc/Hz @ 1 MHz
Frequency drift	5 MHz

4.1 Linewidth Criteria of Optically Generated Carrier

Close to the carrier frequency, the performance of the generated carrier is determined by the linewidth of the optical carrier. The ratio between Equation (4) and (5) gives the single sideband (SSB) phase noise expressed in dBc/Hz [27]. Calculating the SSB phase noise curve for various offset frequencies and comparing it to the values from Table I, one can determine the linewidth of the optical carrier to match the DVB-S requirements. The SSB phase noise of optically generated carrier for offset frequencies up to 1 MHz is plotted in Figure 2 and it is evident that the parameters in Table I shows a Lorentzian

decay of the SSB phase noise. This implies that, for a free running heterodyning system using two lasers, the summed linewidth of the two lasers should be 125 Hz. Moreover, the generated carrier must appear above the noise floor of the heterodyning system. Thus the performance of the carrier is defined by the SSB phase noise (i.e., linewidth) of the laser and must maintain a -110 dBc/Hz phase noise at 1 MHz offset frequency from its center frequency.

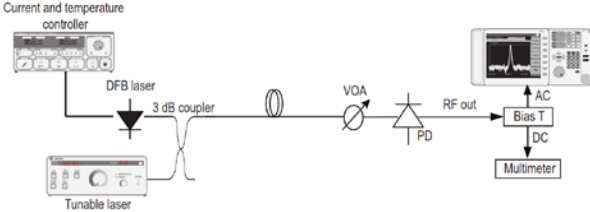


Fig. 4. Power and noise measurement setup. (VOA = variable optical attenuator, PD = photodetector.)

4.2 Carrier-to-noise Ratio Criteria of Photonic carrier

Beyond 1 MHz offset frequency from the carrier carrier, it is the noise floor that determines the system performance. To analyze the impact of noise in this heterodyning system, it is useful to consider all noise sources in the photonic system. The system is affected by noise, comprising thermal noise, shot noise and relative intensity noise (RIN). Assuming that impedance matching has been imposed at the RF detector [28], [29], the total noise PSD can be written as

$$P_N = p_{th} + P_{shot} + P_{RIN}$$

$$= \frac{1}{4} \left(2qI_{av}R_L + 10^{\frac{RIN}{10}} I_{av}^2 R_L \right) \quad (7)$$

where p_{th} is the thermal noise contribution (-174 dBm/Hz in the case where the temperature is 290 K), $q = 1.6 \times 10^{-19}$ C is the electron charge. P_{shot} and p_{RIN} are the shot noise and the RIN contributions, respectively. According to the carrier specifications in Table I, at 1 MHz offset frequency the generated carrier signal has to have less than -110 dBc/Hz phase noise. To keep this value for the optically generated carrier the noise floor must not exceed this limit. To maintain a noise floor of 110 dB below the carrier power, a minimum carrier power is required. Equation (5) shows that the minimum carrier power ultimately sets the minimum laser power in the heterodyning operation.

1) *carrier Power and Noise Measurement: Implementation and Characterization:* In order to investigate the CNR requirement of the optically generated carrier, the carrier power and the contribution of various noise components (i.e., thermal noise, shot noise and RIN) to the noise floor need to be investigated. This investigation involves the measurement of the power of the carrier as well as the noise floor. The block diagram of the experimental setup

to measure the power of the carrier signal and noise in the optical heterodyning scheme is presented in Figure 4. The two lasers used for the optical heterodyning are a DFB laser (Avanex Inc., A1905LMI) and a tunable laser diode (TLD, Santec TSL-210) which have a RIN of -140 dB/Hz and -130 dB/Hz, respectively. The optical signals from both lasers are combined in a 3-dB coupler and then passed through a variable optical attenuator (VOA) before inserting into the PD. The beat signal is provided by a 20 GHz bandwidth photodetector (Discovery Semiconductor DSC30S). A bias-tee (Ortel Co., 100 kHz to 14 GHz) splits off the AC and the DC components of the photo-current. The AC component is measured by an RF spectrum analyzer (RF-SA). The DC photocurrent is measured by a multimeter. The RF-SA measures the PSD of the RF power and the noise floor of the generated carrier. By tuning the VOA it is possible to change the optical power to the PD. This will change both the photo-current and the noise floor. The system noise was characterized for the different photocurrents. The optical power from the DFB laser and the tunable laser were combined and passed through the VOA before inserting into the PD. The VOA was varied from 0 dB to 60 dB with a small step and for each step the total noise power spectral density (PSD) was measured with the RF-SA using the noise marker. The marker was positioned at the frequency of 3.8 GHz and the noise was measured in a 10 kHz noise bandwidth. The marker gave the measured noise power normalized in 1 Hz bandwidth, i.e., in dBm/Hz. As mentioned earlier, the detected photo-current was measured with a multimeter from the DC output of the bias-tee. By inserting the measured value of P_N in Equation (7), the RIN values of the system can be determined. Equation (5) shows that carrier power is proportional to the square of the photocurrent. This relation of carrier power and photo-current is shown in Figure 5(a), indicated by blue solid line. The calculated result is verified by measuring the carrier power for various photo-currents using the setup in Figure 4. Both the measured and calculated carrier power have a slope of 20 dB/dec. Using Equation (7) the total noise power and individual noise contributions are also calculated for various photo-currents and plotted in Figure 5(a). The noise floor is also measured by varying the photo-current using the same measurement setup. Notice that for a photo-current below 0.07 mA the measured noise power is below the displayed average noise level (DANL) of the spectrum analyzer (-166.2 dBm/Hz) of the RF-SA [30]. The noise floor starts increasing above 0.07 mA photo-current and above 0.2 mA of photo-current the RIN noise begins to dominate. As the RIN is proportional to the square of the photo-current, the measured noise floor increases with a slope of 20 dB/dec. Above 0.2 mA of photo-current both the carrier power and noise power have a slope of 20 dB/dec. Further increases in the input optical

power which ultimately increase the photo-current yield no change in the ratio of carrier power and noise power. This makes the CNR as 133 dB at a RIN value of -130 dB/Hz. These experimental values are in good agreement with the calculated values.

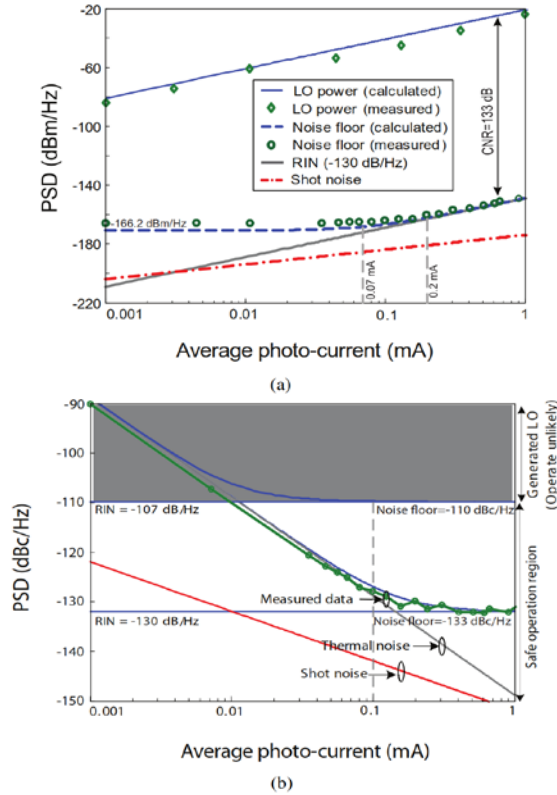


Fig. 5. Comparison of measured and calculated power. (a) generated carrier and noise floor for various photo-currents. (b) noise floor for different values of RIN. The shaded area shows the SSB phase noise of the 125 Hz carrier (-110 dBc/Hz @ 1 MHz) as given in Table 1.

As stated earlier, the phase noise is plotted in the decibel scale. To make better comparison between the phase noise and the noise floor of the heterodyning system, the noise floor needs to be plotted on same scaling as that of the phase noise. In order to express the noise power in decibel scale, the Figure 5(a) is re-plotted with reference to the optically generated carrier power for two RIN values in Figure 5(b). Hence, the PSD plot in dBm/Hz of Figure 5(a) will be transformed to PSD plot in dBc/Hz as a function of the average photo-current. Given in Table 1, at 1 MHz offset frequency the generated carrier should maintain a phase noise of -110 dBc/Hz, this means the noise floor of the system should be below -110 dBc/Hz. In Figure 5(b), with respect to the carrier power the thermal noise, the shot noise and RIN has a slope of -10 dB/dec, -20 dB/dec and 0 dB/dec, respectively. The measured noise floor is very close to the calculated value in Figure 5(b). It is evident from Figure 5(b) that at 0.1 mA average photo-current each laser with a RIN of -107 dB/Hz will keep the total noise floor at -110 dBc/Hz. Above this

photo-current value the CNR will remain constant with higher optical carrier power.

With the help of Equation (5), and assuming the responsivity of the PD (r_{pd}) as 0.8 A/W, the minimum power required for each laser is:

$$P_{L1} = \frac{I_{av}}{2r_{pd}} = \frac{0.2 \times 10^{-3}}{2 \times 0.8} = 0.125 \text{ mW} \quad (8)$$

As the optical power needs to be distributed to each PD of 25 tiles in the PAA, the minimum optical power of each laser required for 25 tiles is 3.1 mW (0.125 mW×25). Finally, the RF output of the PD will be distributed to 64 AE's of each tile, and should be amplified by individual RF amplifier if necessary. Having a minimum optical power of 3.1 mW from a laser with a RIN of -107 dB/Hz, the total noise floor will be at -110 dBc/Hz. This will make the minimum CNR of 110 dB. All these parameters will ensure the optically generated carrier which will maintain a phase noise of -110 dBc/Hz at 1 MHz offset frequency from the carrier frequency.

5. Stabilization of optically generated carrier signals

The frequency of a diode laser depends on the injection current and the temperature and is very sensitive to fluctuations of those parameters. For example, the DFB laser (Avanex inc., A1905LMI) used in our experiment has a frequency sensitivity to injection current and temperature of 325 MHz/mA and 10 GHz/°C, respectively. Several investigations and experiments show that the beat signal generated by a free-running heterodyning system suffers substantial frequency drift [31]. The frequency of a laser generally drifts hundreds of MHz in an ordinary environment [32]. According to the DVB-S specification [26], the maximum allowable frequency drift of the generated carrier is 5 MHz [33]. Therefore, the optically generated carrier needs to be frequency stabilized.

5.1 Optical Frequency Locked Loop Schemes

For the purpose of stabilizing the optically generated carrier, the beat signal is often mixed down to a lower frequency which can be easily processed. One of the main differences among the various optical frequency locking schemes which have been developed in the last decades, is the method used to convert the beat frequency or the downconverted beat frequency to proportional error metric. This error metric controls the frequency of the so-called slave laser maintaining a highly precise frequency offset from a reference laser, labeled as master laser. Previously, a frequency locking approach converted the beat frequency to a proportional voltage by an electronic circuit [34]. The voltage is then compared to a reference voltage

in an electronic comparator, which sets the beat frequency. Another frequency locking scheme uses a frequency divider (prescaler) on the beat frequency to down scale it before processing the error signal [35]. Both of the schemes use active electronic components as frequency to voltage converter (FVC) so it degrades the system dynamics (i.e., loop bandwidth, loop response time). A simple OFLL technique based on the concept presented by Schunemann et al. [36] where an RF discriminator is used as a FVC is proposed. In this discriminator a variable delay line is used as a frequency dependent phase shifter in conjunction with a phase detector to facilitate beat frequency tuning. Our proposed scheme uses all passive RF components (RF power splitter, variable delay line, RF mixer) in the FVC to improve the dynamics of the loop. The block diagram of the proposed OFLL is presented in Figure 6.

5.2 Proposed Optical Frequency Locked Loop Scheme

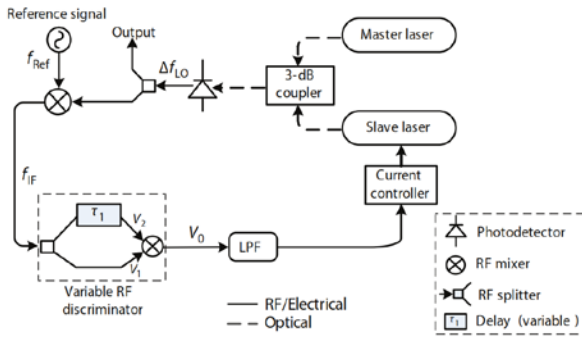


Fig. 6. Proposed optical frequency locked loop (OFLL).

The two lasers used for the experiments are a DFB laser (Avanex inc., A1905LMI) and a tunable laser (TLD, Santec TSL-210). In the experiment the tunable laser and the DFB laser are employed as a master laser and slave laser having optical frequencies f_{ML} and f_{SL} respectively, to produce the beat frequency, $\Delta f_{LO} = f_{ML} - f_{SL}$. The beat signal is provided by a 20 GHz bandwidth photodetector (Discovery Semiconductor DSC30S) and is amplified using a commercial RF amplifier. A power splitter (MiniCircuits ZFRSC-123-S) is used to tap the beat signal for monitoring. The output signal from one of the outputs of the power splitter is mixed with a reference signal, f_{Ref} , at frequency around 10 GHz provided by a signal generator (Agilent PSG E8267D). A downconverted signal, $V_{IF}\cos(2\pi f_{IF}t)$, is produced at the output of the RF mixer (MiniCircuits ZX05-153LH-S) where V_{IF} is the amplitude of the downconverted signal and f_{IF} is the intermediate frequency (IF) given by $f_{IF} = \Delta f_{LO} - f_{Ref}$. The signal is then passed through a variable frequency discriminator. In the frequency discriminator the signal is split into two equal parts by an RF splitter and recombined at a mixer (MiniCircuits SBL 48), after one part has been delayed by a variable delay line (Narda model 3752). Hence,

$$V_1 = \frac{V_{IF}}{2} [\cos(2\pi f_{IF}t)]; V_2 = \frac{V_{IF}}{2} [\cos(2\pi f_{IF}(t - \tau_1))] \quad (9)$$

where V_1 and V_2 are the signals combined in the mixer and τ_1 is the time delay. The resultant signal of the frequency is discriminator at the output of the double balanced mixer (MiniCircuits ZFM-2), V_0 , is [37]

$$V_0 = \frac{V_{IF}}{\pi} [\cos(2\pi f_{IF}\tau_1) + \cos(2\pi f_{IF}(2t - \tau_1)) + \dots] \quad (10)$$

The high-frequency terms (2nd and successive terms between the brackets) are eliminated by a first order low pass filter (LPF) (MiniCircuits SLP-10) with a cutoff frequency, f_c , of 10 MHz. As a result, at the output of the LPF, the output of the RF mixer produces a series of nulls when $f_{IF} = (2n + 1)/4$, where $n = \pm 0, \pm 1, \pm 2 \dots$. The feedback system acts on the slave laser injection current and allows to actively control the emission frequency of the slave laser, so that a constant frequency difference between the slave laser and the master laser is maintained. The frequency of the slave laser is maintained. The frequency of the slave laser is tuned by applying an external voltage to its injection current controller (ILX Lightwave LDC-3724).

5.3. Characterization of the components

From the schematic of the proposed OFLL (in Figure 6), one can notice that the dynamics of the loop will be influenced by the characteristics, namely the frequency response and the conversion factor, of the various components used in the loop. In this section the characteristics of the FVC is investigated. The discriminator signal at the output of the LPF as a function of the beat frequency for a delay of $\tau_1 = 3$ ns is shown in Figure 7.

The delay of 3 ns was realized by using a passive RF component, namely a phase shifter (Narda model 3752). As shown in this figure, the OFLL allows stable locking to several values of the nulls which are spaced by $1/\tau_1$ corresponding to the zero crossings of the error signal. The difference in frequency (offset) between the first null (the point where the beat frequency being locked) from the reference frequency is given by

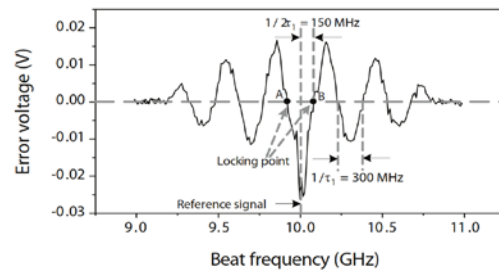


Fig. 7. Beat frequency as a function of error voltage for a delay of $\tau = 3$ ns. The beat signal is locked to an offset from the reference signal.

$$\Delta f = \frac{1}{2\tau_1} \quad (11)$$

The purpose of the RF discriminator used in the OFLL is to convert the frequency to its input to a proportional voltage. The frequency-to-voltage conversion factor, K_d , for the frequency discriminator is maximum at the closest nulls to the reference frequency (point A and B in Figure 7) and is calculated to be 0.15 mV/MHz for a delay of $\tau_1 = 3$ ns. From Equation (11), a higher delay will reduce the frequency offset of the null from the reference frequency and will increase the slope at the nulls which ultimately will give a higher conversion of K_d .

The various parameters and their values used in our analysis are summarized in Table 2.

Table 2: Various loop parameters

Parameter	Value	Dimension	Notation
Responsivity of the PD	0.8	A/W	r_{pd}
Conversion loss of the mixer	-5.5	dB	K_{mix}
Total gain of the RF amplifiers	variable	dB	K_a
Frequency-to-voltage conversion factor of the RF discriminator	0.15	mV/MHz	K_{FVC}
Resonance frequency of the current controller of the slave laser	425	kHz	f_r
Cut-off frequency of the current controller of the slave laser	1	MHz	F_c
Voltage-to-frequency conversion factor of the current controller	6.5	MHz/mV	K_{SL}

5.4 Optical Frequency Lock Loop Analysis

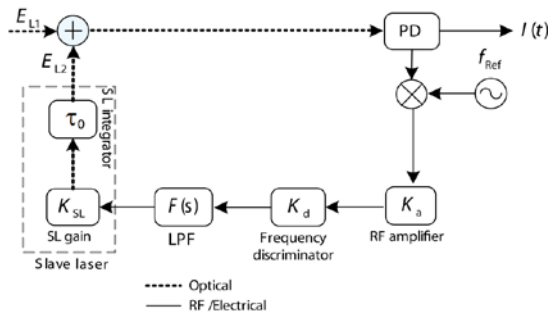


Fig. 8. Linearized s-domain representation of the OFLL

The proposed OFLL in Figure 6 can be represented in a generic model for a feedback system and presented as Laplace domain (s-domain) representation [38] of OFLL in Figure 8.

In Figure 6, the optical and the electrical connections are represented by dotted and solid lines, respectively. The optical field from the master and the slave laser are

represented by E_{L1} and E_{L2} , respectively. The fields are combined and inserted in a PD. The gain of the PD can be defined as $K_{pd} = r_{pd}$ where r_{pd} is the responsivity of the PD. The output beat frequency from the PD is mixed with a reference frequency, f_{Ref} . The RF mixer has a conversion loss of K_{mix} . The downconverted signal is then amplified by an RF amplifier with a gain of K_a . An RF frequency discriminator converts the frequency to its proportional voltage with a conversion factor of K_{FVC} . The error voltage is passed through a LPF to filter out the high frequency components and is then applied to the current controller of the slave laser. The slave laser acts as a current-controlled oscillator and the change in output optical frequency is a function of the frequency components of the input current modulation. The frequency response of the current controller is indicated by $F_{FM}(f)$ and its Laplace transform is denoted by $F_{FM}(s)$. The external voltage-to-frequency conversion factor is denoted by K_{SL} . As shown earlier the bandwidth of the current controller will dominate in the loop so its frequency response will be considered in the s-domain model.

From the linearized s-domain representation of the OFLL the closed-loop transfer function of the OFLL is [38]

$$H(s) = \frac{4\pi^2 f_n^2}{s^2 + s\zeta 2\pi f_n + 4\pi^2 f_n^2 \left(1 + \frac{1}{K}\right)} \quad (12)$$

where $K = K_{pd}K_{mix}K_aK_{FVC}K_{SL}$ is the total gain and f_n and ζ represent the natural frequency and the damping factor of the loop, respectively. is expressed by following equations [38]:

$$\zeta = \frac{f_c}{f_n} \quad (13)$$

$$f_n = f_r \sqrt{K} \quad (14)$$

5.5 Experimental Results

In this section the frequency stability and loop response of the OFLL will be investigated. Like any feedback system the dynamics of these functionalities are determined by various parameters (i.e., loop natural frequency and damping factor), will also be investigated.

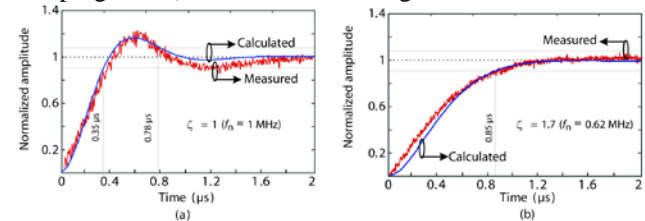


Fig. 10. Loop settling time comparison on calculated and measured values for various damping factors, ζ , using step response. (a) damping factor $\zeta = 1$ (b) damping factor $\zeta = 1.7$.

1) Loop Response Time: The experimental setup for step response measurement is shown in Figure 9. The response of the OFLL can be measured by disturbing the current

controller of the slave laser (DFB laser) with a step signal from a vector signal generator (Agilent PSGE8267D) and simultaneously by measuring the resulting response at the output of the LPF. The step signal will introduce an external disturbance in the loop and the optically generated carrier signal will suffer from a temporal deviation from the desired frequency due to this temporal instability, also called ringing. Soon after the disturbance the loop will eventually bring the system in former stable condition. The recovery duration of the generated carrier signal from its unstable condition is measured by an oscilloscope (Agilent infinium 54854A). For accurate measurement the oscilloscope and the vector signal generator are synchronized by an external trigger.

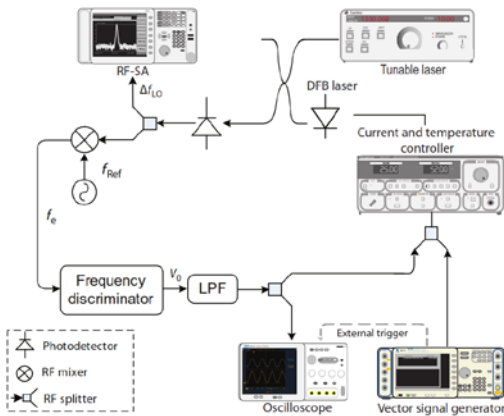


Fig. 9. Loop response time measurement setup.

Employing the the values of parameters in Table 2, for a given values of gain, $K_a = 14$ dB, the natural frequency, f_n , and the damping factor, ζ , can be calculated using Equation (13) and (14) as 1 MHz and 1, respectively. For $K_a = 10$ dB the calculated values of the natural frequency and the damping factor becomes $f_n = 0.62$ MHz and $\zeta = 1.7$, respectively. From Figure 10, for $\zeta = 1$ and $\zeta = 1.7$ the speed of the response of the loop is measured to be $0.35 \mu s$ and $0.85 \mu s$, respectively. From Figure 10(a) it is evident that for a value of $\zeta = 1$ the calculated loop settling time is found to be $0.78 \mu s$ which become slower to $0.58 \mu s$ (Figure 10(b)) for $\zeta = 1.7$ (so called critical damping). The experimental results are in good agreement with the calculated values. From Figure 10 we can observe that there is a trade-off between the loop response time and settling time. With higher damping factor, the loop response time increases with decrease of settling time. The optimum value of damping factor can be indicated as $\zeta = 1$ where both the loop response time and settling time is also optimum. The optimized loop natural frequency, f_n , is 1 MHz.

2) *Optimum Choice of the Loop Parameters:* In order to achieve an optimum performance of an OFLL, various loop parameters should be chosen properly. In the

previous section it is experimentally demonstrated that the dynamics of an OFLL is very much influenced by proper choice of the damping factor of the loop which is ultimately determined by bandwidth, natural frequency and gain of the loop. Using Equation (13) and (14), the relation of the bandwidth, the natural frequency and the gain of the OFLL is shown in Figure 11. It is evident from Figure 11, for a given bandwidth of the loop, as in the case of our OFLL, the loop natural frequency increases with increase of the gain. As a consequence the damping factor of the loop will also change. For instance, for a loop bandwidth of 1 MHz, the loop natural frequency is 1 MHz for a gain of 14 dB and $\zeta = 1$ which decreases to 0.62 MHz for a gain of 10 dB and $\zeta = 1.7$.

Various loop parameters (i.e., loop natural frequency, gain) and the damping factor was determined keeping on mind the limitation of bandwidth of the proposed OFLL. However, for a stable feedback system an optimum value of the damping factor should be chosen first and from it one should determine the optimum values of the loop bandwidth, natural frequency and gain using Equation (13) and (14).

3) *Frequency Stability of the OFLL:* Finally, the optimized loop parameters are addressed and are used to demonstrate the frequency stability of the beat spectrum for both free running and OFLL technique for more than ten hours as shown in Figure 12. The following loop parameters (Table 3) are used to evaluate the frequency stability of our OFLL:

Table 3: Loop parameters for stability evaluation

Parameter	Value	Notation
Amplifier gain	14 dB	K_a
Damping factor	1	ζ
Loop bandwidth	1 MHz	f_{BW}

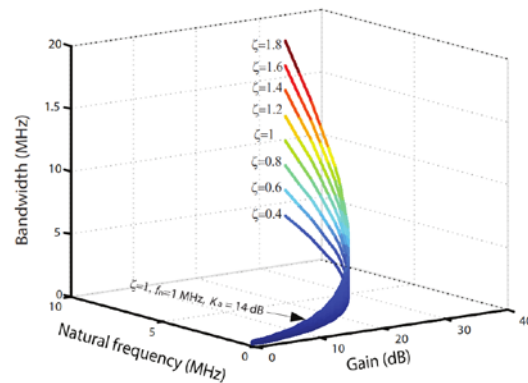


Fig. 11. Relation of bandwidth, natural frequency and gain of an OFLL. Plots are shown for various damping factors.

Figure 12 shows that the free-running beat spectrum suffers a frequency drift of 600 MHz in 13 hours duration.

A 9.6 GHz reference signal locks the optically generated carrier signal at 9.75 GHz and stabilizes the generated carrier signal. As indicated in the inset of Figure 12 the short term (in seconds) frequency stability of both free-running and locked frequencies are 20 MHz and 0.4 MHz, respectively. Figure 7 shows that the capture range of the OFLL is 150 MHz, much larger than 20 MHz frequency drift of the free running carrier signal, which prevents the feedback loop from hopping between different locking points. Both the long term (more than 10 hours) and the short term (in seconds) frequency stability of the OFLL show very similar stability. Hence the system shows optimized performance in terms of frequency stability.

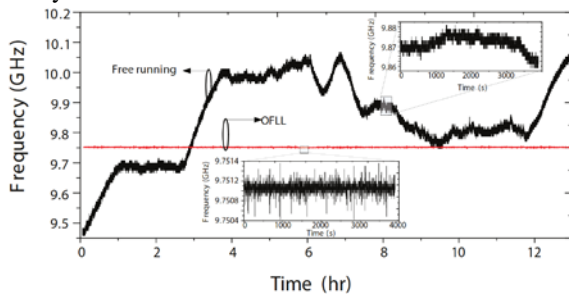


Fig. 12. Frequency stability evaluation of free-running and OFLL scheme at 10 GHz beat frequency, measured with the setup described in Figure 6.

6. Conclusions

The optical carrier generation by OFLL to comply with the requirements of the standard carrier used in commercial LNBS has been investigated. The detailed analysis of the OFLL scheme is presented. Specifications requirement on carrier power, linewidth and relative intensity noise of the optical carrier have been addressed. The optical carrier generation is experimentally demonstrated and the requirements on CNR have been determined by measuring the noise floor and the optical carrier power. The measured values are compared with the calculated values and found to be very close. To achieve an optical carrier whose performance would be comparable to a standard carrier its linewidth should be 125 Hz. Also the laser RIN should be -123 dB/Hz or lower with a minimum optical power of 3.1 mW. Due to the strict requirements of the stability of the optically generated carrier our demonstrated frequency locked technique is able to stabilize the carrier within ± 4 MHz with a settling time of 11.5 μ s.

Acknowledgments

This work is in the framework of the MEMPHIS project. The authors gratefully acknowledge the support of the Smart Mix

Programme of the Netherlands Ministry of Economic Affairs and the Netherlands Ministry of Education, Culture and Science.

References

- [1] A. Meijerink, C. G. H. Roeloffzen, R. Meijerink, L. M. Zhuang, D. A. I. Marpaung, M. J. Bentum, M. Burla, J. Verpoorte, P. Jorna, A. Hulzinga, and W. van Etten, "Novel ring resonator-based integrated photonic beamformer for broadband phased array receive antennas-part I: design and performance analysis," *J. Lightw. Technol.*, vol. 28, no. 1, pp. 3–18, 2010.
- [2] C. O. Adler, D. J. Van Aalen, R. S. Carson, A. F. Morrison, M. E. Lavelle, E. D. Anderson, G. R. Onorati, and J. K. Cunningham, "Airborne reception of data and direct broadcast TV using a phased array antenna," in *Proc. IEEE Int. Conf. on Phased Array Sys. and Tec.*, 2000, pp. 223–226.
- [3] D. Marpaung, L. Zhuang, M. Burla, C. Roeloffzen, J. Verpoorte, H. Schippers, A. Hulzinga, P. Jorna, W. Beeker, A. Leinse, R. Heideman, B. Noharet, Q. Wang, B. Sanadgol, and R. Baggen, "Towards a broadband and squint-free K_u -band phased array antenna system for airborne satellite communications," in *Proc. 5th European Conf. on Antennas and Prop. (EuCAP)*, Apr. 2011, pp. 2623–2627.
- [4] S. Fikar and A. L. Scholtz, "Novel low-cost antenna array for vehicular reception of K_u -band satellite television," in *IEEE Antennas and Prop. Society Int. Symp. (AP-S)*, 2008, pp. 1–4.
- [5] R. Baggen, S. Vaccaro, and D. L. del Rio, "Design considerations for compact mobile K_u -band satellite terminals," in *Proc. of the Second European Conf. Antennas and Prop. (EuCAP)*, 2007, pp. 1–5.
- [6] F. Yoshiyuki, S. Masaki, N. Seiji, T. Shinichi, O. Yutaka, W. Eiji, S. Manabu, T. Yukio, and K. Tetsuya, "Development of helicopter satellite communication system for the disaster information transmission," *IEICE Trans. on Commun.*, vol. J91-B, no. 12, pp. 1611–1619, 2008.
- [7] M. Skolnik, *Introduction to Radar Systems*, 2nd ed. McGraw-Hill, 1962.
- [8] M. L. VanBlaricum, "Photonic antenna reconfiguration: a status survey," in *Proc. of the SPIE, Photonics and Radio Freq. II*, vol. 3463, pp. 180–189.
- [9] S. Ayotte, A. Babin, P. Poulin, M. Poulin, A. Jeanneau, M. J. Picard, D. Poulin, C. A. Davidson, Aube, x, M., I. Alexandre, F. Costin, F. Pelletier, J. F. Cliche, Te, M. tu, and B. Shillue, "Laser synthesizer of the ALMA telescope: design and performance," in *Proc. IEEE Int. Topical Meeting Microwave Photonics (MWP)*, 2010, pp. 249–252.
- [10] J. M. Payne and W. P. Shillue, "Photonic techniques for local oscillator generation and distribution in millimeter-wave radio astronomy," in *Proc. IEEE Int. Topical Meeting Microwave Photonics (MWP)*, 2002, pp. 9–12.
- [11] J. T. B. C. D. V. Y. Q. Reul, N. and Y. H. Kerr, "SMOS satellite LLLLLL band radiometer: a new capability for ocean surface remote sensing in hurricanes," *J. of Geophysical Res.*, 2011.

- [12] A. Chenakin, "Phase noise reduction in microwave oscillators," *Microwave J.*, vol. 52, no. 10, pp. 124–140, 2009.
- [13] O. Solgaard, J. Park, J. B. Georges, P. K. Pepeljugoski, and K. Y. Lau, "Millimeter wave, multigigahertz optical modulation by feedforward phase noise compensation of a beat note generated by photomixing of two laser diodes," *IEEE Photon. Technol. Lett.*, vol. 5, no. 5, pp. 574–577, 1993.
- [14] Z. Deng and J. Yao, "Photonic generation of microwave signal using a rational harmonic mode-locked fiber ring laser," *IEEE Trans. Microw. Theory Tech.*, vol. 54, no. 2, pp. 763–767, 2006.
- [15] I. G. Insua, D. Plettemeier, and C. Schaffer, "Simple remote heterodyne radio-over-fiber system for gigabit per second wireless access," *J. Lightw. Technol.*, vol. 28, no. 16, pp. 2289–2295, 2010.
- [16] K. H. Lee, W. Y. Choi, Y. A. Leem, and K. H. Park, "Harmonic millimeter-wave generation and frequency up-conversion using a passively mode-locked multisection DFB laser under external optical injection," *IEEE Photon. Technol. Lett.*, vol. 19, no. 2-4, pp. 161–163, 2007.
- [17] C. Williams, F. Quinlan, and P. J. Delfyett, "Injection-locked modelocked laser with long-term stabilization and high power-per-combine," *IEEE Photon. Technol. Lett.*, vol. 21, no. 2, pp. 94–96, 2009.
- [18] G. Santarelli, A. Clairon, S. N. Lea, and G. M. Tino, "Heterodyne optical phase-locking of extended-cavity semiconductor lasers at 9 GHz," *Opt. Communications*, vol. 104, no. 4-6, pp. 339–344, 1994.
- [19] J. P. Yao, "Microwave photonics," *J. Lightw. Technol.*, vol. 27, no. 1-4, pp. 314–335, 2009.
- [20] G. Ritt, G. Cennini, C. Geckeler, and M. Weitz, "Laser frequency offset locking using a side of filter technique," *Appl. Phys. B-Lasers and Optics*, vol. 79, no. 3, pp. 363–365, 2004.
- [21] E. H. Bernhardt, H. A. G. M. van Wolferen, L. Agazzi, M. R. H. Khan, C. G. H. Roeloffzen, K. Worhoff, M. Pollnau, and R. M. de Ridder, "Ultra-narrow-linewidth, single-frequency distributed feedback waveguide laser in $\text{Al}_2\text{O}_3:\text{Er}^{3+}$ on silicon," *Opt. Lett.*, vol. 35, no. 14, pp. 2394–2396, 2010.
- [22] M. R. H. Khan, M. Burla, C. G. H. Roeloffzen, and D. A. I. Marpaung, "Phase noise analysis of an RF local oscillator signal generated by optical heterodyning of two lasers," in *Proc. of the 14th Annual Symp. of the IEEE Photonics Benelux Chapter*, 2009, pp. 161–164.
- [23] C. Lennartz, W. van Etten, T. van Osch, and F. Huijskens, "Laser spectra measured with the recirculating self heterodyne technique," *J. Opt. Commun.*, vol. 17, no. 4, pp. 138–146, Aug. 1996.
- [24] E. Ip, A. P. T. Lau, D. J. F. Barros, and J. M. Kahn, "Coherent detection in optical fiber systems," *Opt. Exp.*, vol. 16, no. 2, pp. 753–791, Jan. 2008.
- [25] G. P. Agrawal, *Fiber-Optic Communication Systems*. New York: John Wiley & Sons, 1997.
- [26] "Digital video broadcasting (DVB): Interaction channel for satellite distribution systems; guidelines for the user (EN 301 790)." [Online]. Available: <http://www.dvb.org/technology>
- [27] F. Gardner, *Phaselock Techniques*. Wiley, 2005.
- [28] C. H. Cox, *Analog Optical Links : Theory and Practice*. Cambridge University Press, 2004.
- [29] D. Marpaung, C. Roeloffzen, A. Leinse, and M. Hoekman, "A photonic chip based frequency discriminator for a high performance microwave photonic link," *Opt. Exp.*, vol. 18, no. 26, pp. 27 359–27 370, 2010.
- [30] "Spectrum analysis basics: Application note 150, Agilent Technologies, Inc, USA." [Online]. Available: <http://cp.literature.agilent.com/litweb/pdf/5952-0292.pdf>
- [31] F. Friederich, G. Schuricht, A. Deninger, F. Lison, G. Spickermann, P. H. Bolivar, and H. G. Roskos, "Phase-locking of the beat signal of two distributed-feedback diode lasers to oscillators working in the MHz to THz range," *Opt. Exp.*, vol. 18, no. 8, pp. 8621–8629, 2010.
- [32] D. H. Yang and Y. Q. Wang, "Preliminary-results of an optically pumped cesium beam frequency standard at peking university," *IEEE Trans. On Instrumentation and Measurement*, vol. 40, no. 6, pp. 1000–1002, 1991.
- [33] E. Casini, R. D. Gaudenzi, and A. Ginesi, "DVB - S2 modem algorithms design and performance over typical satellite channels," *Int. J. Satellite Commun. and Net.*, vol. 22, no. 3, pp. 281–318, 2004.
- [34] T. Stace, A. N. Luiten, and R. P. Kovacich, "Laser offset-frequency locking using a frequency-to-voltage converter," *Measurement Sci. Technol.*, vol. 9, no. 9, pp. 1635–1637, 1998.
- [35] A. Castrillo, E. Fasci, G. Galzerano, G. Casa, P. Laporta, and L. Gianfrani, "Offset-frequency locking of extended-cavity diode lasers for precision spectroscopy of water at 1.38 μm ," *Opt. Exp.*, vol. 18, no. 21, pp. 21 851–21 860, 2010.
- [36] U. Schunemann, H. Engler, R. Grimm, M. Weidemuller, and M. Zielonkowski, "Simple scheme for tunable frequency offset locking of two lasers," *Rev. Sci. Instr.*, vol. 70, no. 1, pp. 242–243, 1999.
- [37] B. G. Chris Toumazo, George S. Moschytz, Ed., *Trade-Offs in Analog Circuit Design: The Designer's Companion*, 2002nd ed. Kluwer, 2004.
- [38] D. R. Stephens, *Phase-locked loops for wireless communications: digital, analog, and optical implementations*, 2nd ed. Kluwer, 2001.